ELSEVIER

Sensors and Actuators A 102 (2002) 165–175

SENSORS AND ACTUATORS A PHYSICAL

www.elsevier.com/locate/sna

Micromachined optical waveguide cantilever as a resonant optical scanner

Wei-Chih Wang[a,*], Mark Fauver[b], Joe Nhut Ho[a], Eric J. Seibel[a,b], Per G. Reinhall[a]

[a]*Department of Mechanical Engineering, University of Washington, Seattle, WA 98195, USA*
[b]*Human Interface Technology Laboratory, University of Washington, Seattle, WA 98195, USA*

Received 12 March 2002; accepted 12 August 2002

Abstract

Design, fabrication, and testing of a micromachined cantilever beam that is optically transmissive and operates in the resonant mode is presented with application as a micro-optical scanner. An optical waveguide is formed from a 2.2 μm thick SiO_2 layer deposited on a single crystal silicon wafer and etched to yield a SiO_2/Si composite slab cantilever. Using a novel capacitively coupled reactive ion etching (RIE) technique, a cavity is back-etched in the silicon to release the 30–40 μm thick and 0.5–1.5 mm long cantilevers from the wafer. An etch rate of 2.0–2.2 μm/min in Si, an anisotropy of 0.5 and selectivity to thermal oxide (Si:SiO_2 = 10:1) and to photoresist (Si:+PR = 8.6:1) are reported. Evaporated aluminum film is used as a passivation material. Optical and mechanical tests are performed on these microfabricated structures. The first mode resonances are found between 16 and 52 kHz with response amplitudes ranging from 62.5 to 420 μm. Optical throughput was estimated at 10 nW, but this was greatly diminshed due to scattering losses, primarily at the edges of the waveguide. Since cantilever waveguides with resonant frequencies above 20 kHz are potentially suitable for video rate scanning, these devices maybe used for image acquisition and display.

© 2002 Elsevier Science B.V. All rights reserved.

Keywords: Waveguide; Optical scanner; Cantilever

1. Introduction

The goal of the proposed integrated optical device is to use existing microfabrication technology to create a more compact, integrated system for wide field-of-view and high-resolution image display and acquisition. Using MEMS fabrication processes allows for the integration of light source, scanner, actuators, sensors, detectors and electronics on a single chip configuration. This reduces the overall size and the power consumption of the system, while potentially improving the signal to noise ratio and image resolution. Batch processing also can guarantee a more consistent product, low cost in manufacturing and making disposable medical imaging devices possible.

Conventional image acquisition systems such as flexible endoscopes and boroscopes sample an image plane using a bundle of optical fibers in registration with the pixels on a camera. The approach is limited by the overall diameter of the fiber bundle and the number of pixel detectors on a CCD camera. In order to create a more flexible and less invasive endoscope while preserving image quality, the diameter of endoscopes must be reduced. Currently, reducing the diameter of endoscopes reduces the possible number of pixels, and thus reduces the resolution and/or field of view (FOV) of the device. According to the prior work [1,2] an optical fiber can be used as a scanning waveguide which resonates to scan emitted light at its distal end. The image is generated by collecting the back-scattered light using a light detector. With the reduction of the system to a single microfabricated waveguide cantilever, the overall size is reduced and resolution and FOV are maintained.

1.1. Design

The concept of a micromachined scanning optical microscope has been explored in the form of confocal scanning microscope design that employs a resonant *XY* bimorph stage [3], a resonant cantilever probe and lens [4], or at least one resonant micromirror [5,6]. The confocal design

* Corresponding author. Tel.: +1-206-543-2479; fax: +1-206-685-8047.
E-mail address: abong@u.washington.edu (W.-C. Wang).

0924-4247/02/$ – see front matter © 2002 Elsevier Science B.V. All rights reserved.
PII: S0924-4247(02)00303-5

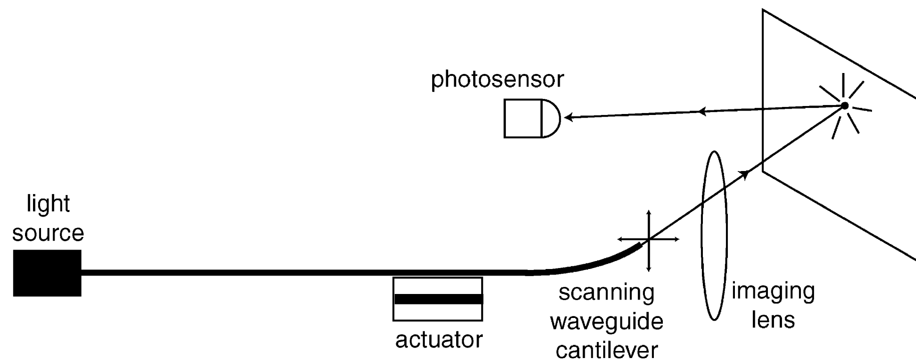

Fig. 1. A schematic of a microimage acquisition device illustrating the components of light source, actuator, optical scanner, lens, and detector. The light spot diameter on the illumination plane, not the photosensor size, limits the image resolution. Note, a micro-optical display would use a light source modulated in synchronization with the scanner, and not use a detector.

for image acquisition has the advantage of spatially filtering the back-scattered light while using the same optical fiber for illumination and signal collection. However, the extremely low efficiency of light collection (into the core diameter, typically 4 μm) of this design remains a disadvantage. An alternative approach is to use a microfabricated scanning optical waveguide for illumination only, with one or more photosensors with larger collection efficiencies for image acquisition (Fig. 1). High image resolution is preserved because the illuminated spot size rather than the photosensor size determines the pixel resolution. Unlike commercial optical endoscopes, the detector size does not affect the acquired image resolution [1]. Image resolution and FOV can be changed dynamically by electronically changing the scanning amplitude and/or the sampling rate of the light detector.

The design, fabrication, and testing of the major component of our scope design, the resonant waveguide scanner, is described in this report. The device structure we have employed for the optical scanner is a simple two-layer composite slab waveguide. The SiO_2 layer is used for the optical "core" through which the visible light will travel. Due to the less than desirable mechanical properties of thermal oxide, another layer formed of silicon gives the cantilever increased mechanical stiffness and durability. Because silicon has a high index of refraction and is absorbing in the visible band (i.e. $n \sim 3.85(1\text{-}0.02j)$ at 632 nm) [7], it is recommended to use a low index buffer layer to isolate the silicon substrate from the waveguide. However, for simplicity the low index buffer layer was eliminated from the design with the rationale that over the short length of the waveguide (<2 mm) optical power losses would be acceptable.

Fabrication of the waveguide cantilever is completed as shown in Fig. 2. Although several dielectric materials were considered for the micromechanical waveguide, thermal oxide ($n = 1.46$ at $\lambda = 600$ nm) was chosen as the waveguide structure. To facilitate coupling of incident light into the waveguide from a singlemode optical fiber, a U-shaped groove was etched in the silicon.

A variety of fabrication techniques for the silicon and SiO_2 cantilever beams have been reported in the literature [8–13]. Common techniques used in the process are back etching, dopant-dependent etch stop, anodic oxidation etch stop, electrochemical etch stop and surface etching using silicon dioxide as an etch mask. To form a cantilever beam structure, aqueous solutions (such as KOH, EDP, NaOH or TMAH) are used in anisotropic etching of silicon. These methods suffer from crystal orientation dependent etching. Other problems such as rounded corners and undercut sidewalls occur in wet chemical etching. Anisotropic etching also makes it impossible to form a flat vertical wall at the end

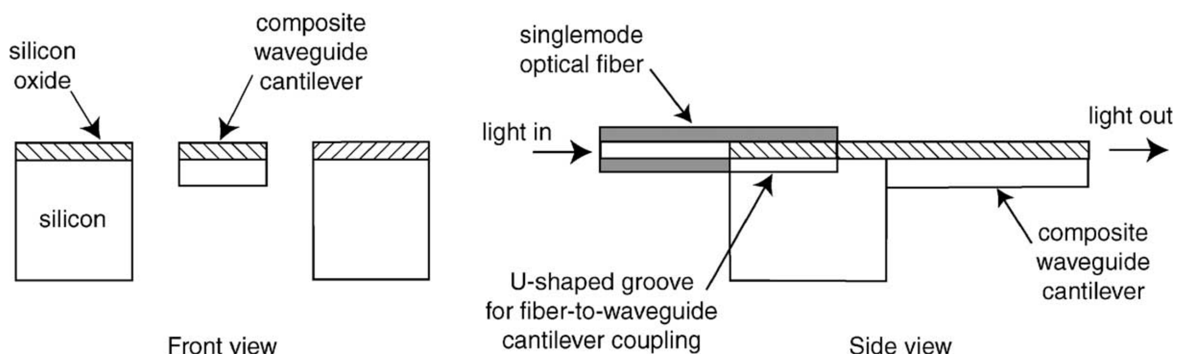

Fig. 2. Schematic of the Si/SiO_2 resonant waveguide scanner.

of the coupler because of the slow etching {1 1 1} plane on a ⟨1 0 0⟩ wafer. Furthermore, the dielectric materials we considered for the optical waveguiding layer such as SiO_2, spin on glass (SOG) and spin on polymer (SOP) will not survive in some of the alkaline solutions (e.g. KOH), thus motivating us to develop a new etching method using a reactive ion etching (RIE) process. Our bulk micromachining technique is unique in that beam structures are released using conventional parallel plate RIE system, whereas typical bulk micromachining technique can only be done in DRIE process [14]. Normally parallel plate RIE is used only in forming the waveguide pattern. The beams are still obtained by either subsequent wet etching or wafer bonding [12,15,16].

The uniqueness of the process is that a high etch rate (2.2 μm/min) and a high aspect ratio (∼1500 μm × 100 μm × 40 μm) is achieved using conventional parallel plate type of RIE instead of ICP or ECP type of reactors. The process creates a fairly sharp edge and little undecutting on both silicon and oxide. The technique is compatible to many dielectric materials that might be used for waveguides. The major challenges in using RIE of bulk silicon are finding an etch mask material which can withstand the gas used in the process for a long duration, and a recipe which produces a relatively fast etch rate, good anisotropy and good selectivity. After searching through a few available metals and photoresists for the passivation materials, aluminum turns out to be the best choice. Its non-reactive and non-catalytic characteristic to SF_6 and CHF_3 gases and its availability make it an ideal material for the mask.

2. Methods

2.1. Fabrication

Starting with a 3 in. double-sided double-polished ⟨1 0 0⟩ oriented, p-type (approximately 400 μm thick) silicon wafer, a 2 μm thick oxide film is thermally grown at 1050 °C using a wet thermal oxidation process (Fig. 3a, oxygen bubbled through a water bath at 95 °C). This process is chosen for its growth rate and relatively low residual stress [17,18]. A slow cooling process, in this case at a rate of 2 °C/min, was also enforced to insure a lower oxide stress buildup. This layer functions as the optical waveguiding layer.

Immediately after cooling, a layer of aluminum is evaporated on the bottom side of the wafer to form the masking layer for the subsequent RIE (Fig. 3b). A 1000 Å thick layer of aluminum is used to prevent metal lift-off during the long silicon etch in RIE [19]. After covering the front and back surface with a thick layer of AZ4620 photoresist (∼10 μm), the front and back mask patterns are aligned and exposed using an aligner (ABM) and then developed (Fig. 3c).

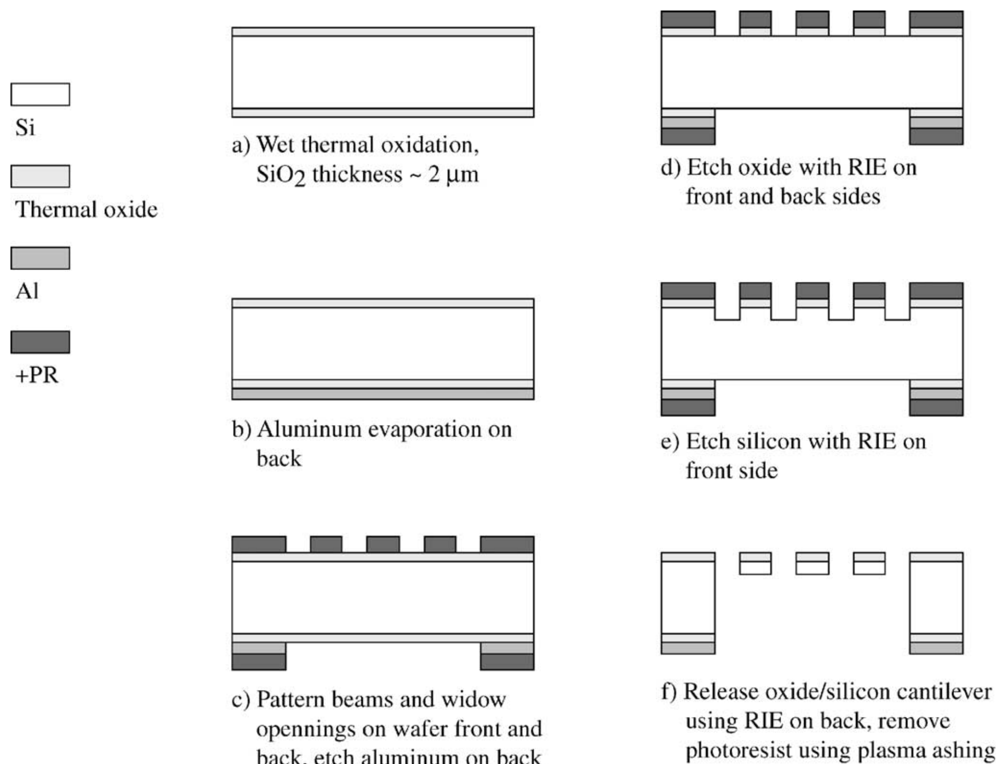

Fig. 3. Fabrication steps for the manufacture of Si/SiO_2 waveguide cantilevers: (a) wet thermal oxidation, SiO_2 thickness ∼2 μm; (b) aluminum evaporation on back; (c) pattern beams and widow openings on wafer front and back, etch aluminum on back; (d) etch oxide with RIE on front and back sides; (e) etch silicon with RIE on front side; (f) release oxide/silicon cantilever using RIE on back, remove photoresist using plasma ashing.

Next the front and back side oxide are etched. The back side is done first to protect the front side pattern. They are anisotropically etched in the Trion Phantom RIE reactor with settings of 45 standard cubic cm per minute (sccm) CHF_3 and 2 sccm O_2, at 80 mTorr and 70 W of power (Fig. 3d). The average etch rate is measured at 150 Å/min for the oxide. Selectivity between photoresist and silicon oxide is about 2:1. Etching is stopped when the silicon is reached. Buffered hydrofluoric acid wet etching to pattern the oxide was not used because the acid produces an isotropic etching of SiO_2. This undercutting of the oxide beneath the masking layer is due to isotropic etching and this is not desirable for the narrow beam structures.

The silicon substrate is then etched down anisotropically for approximately 40 μm (Fig. 3e) using RIE settings of 50 sccm SF_6, 8 sccm O_2, 4 sccm CHF_3, 120 mTorr, and 100 W. The aluminum mask is sufficient to protect the oxide for up to a 400 μm deep silicon etch. The resulting etch rate of 2.0 μm/min is comparable to 1–3 μm/min [20] from the standard ICP deep ion etching process. This process etches out the profile of the cantilever and produces the U-shaped groove used for guiding the coupling of an optical fiber to the cantilever waveguide (Fig. 5).

A final RIE etch (50 sccm SF_6, 200 mTorr, 100 W) from the back side releases the cantilever beams (Fig. 3f). The average etch rate is found to be ~2.2 μm/min. Etch selectivity between oxide and silicon is 1:10, and 1:8.6 between photoresist and silicon. Anisotropy $A \sim 0.5$ ($A = 1 - V/H$, where $V =$ horizontal undercut, $H =$ etch depth) is observed (Fig. 4). Remaining photoresist is removed using plasma ashing.

Pictures of the microfabricated device are shown in Fig. 5. The cantilever beams have an uniform width of 100 μm and vary in length from 0.5 to 1.5 mm. The U-groove coupler (Fig. 5c) has a width of 125 μm and a depth of 40 μm.

2.2. Optical testing

To couple light into the fabricated optical waveguide cantilevers, an apparatus (Fig. 6) was constructed consisting of a tilt adjustment for the light-carrying fiber, an *XYZ* positioning stage to accurately place the fabricated part for end-butting of the optical fiber to the tapered waveguide coupler. A microscope (6.3× objective, 10× eyepiece) was used to aid alignment of the optical fiber to the microfab structure. A second microscope (43× objective, 10× eyepiece) was used to image the light transmitted out the optical waveguide cantilever end. Due to problems experienced in using the U-shaped groove to couple light into the optical waveguide cantilever, the microfabricated part was cleaved in the middle of the tapered waveguide coupler to aid in butt-end coupling.

The cleaved end of a single mode optical fiber was then positioned using the tilt mechanism to be parallel to the waveguide and perpendicular to the cleaved edge. A 10 mW 635 nm laser diode (made by Melles Griot) was coupled into the single mode fiber. Using the two microscopes shown in Fig. 6 for guidance, light coupling was attained for the microfabricated waveguide cantilevers.

2.3. Mechanical testing

The wafer consisting of microfabricated devices was cleaved into sections, and a single section consisting of a trio of cantilevers was mounted to a piezoelectric bimorph

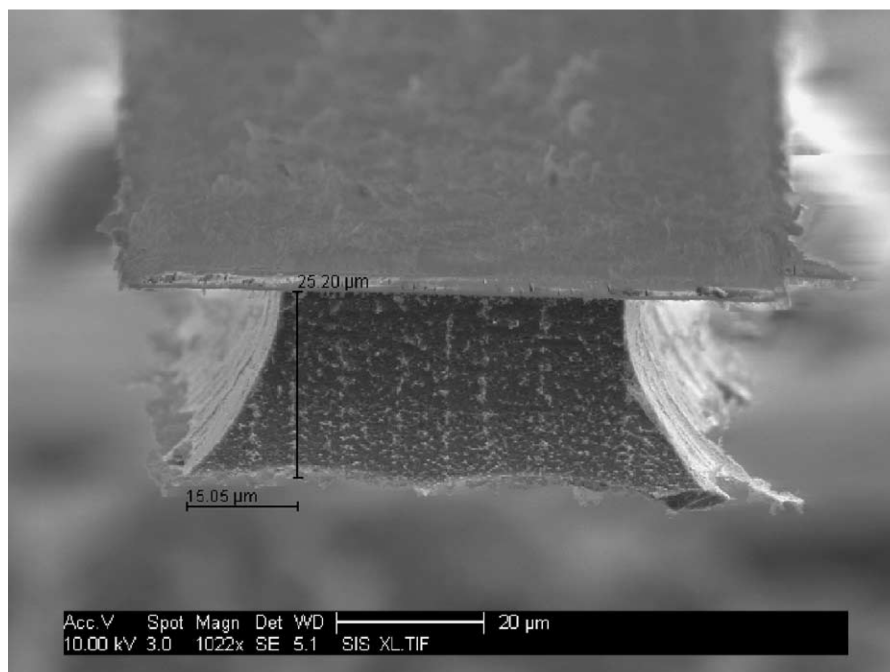

Fig. 4. SEM micrograph of the tip of the silicon/silicon oxide beam.

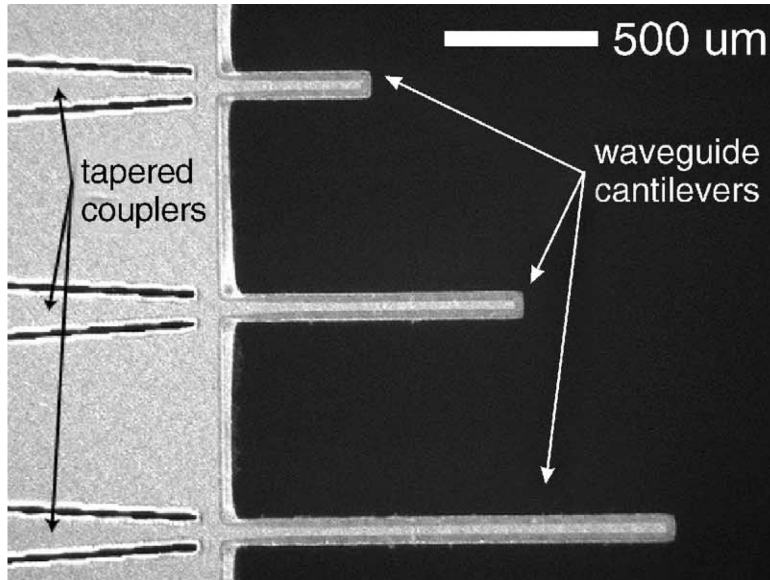

(a)

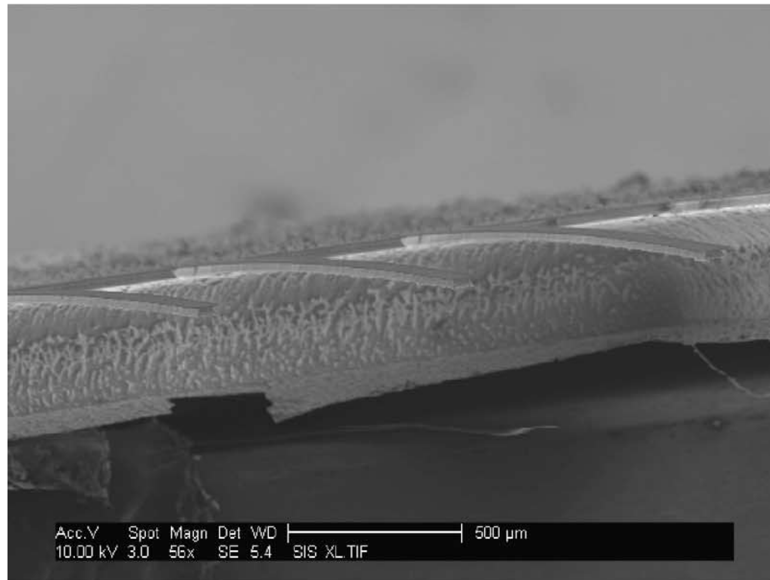

(b)

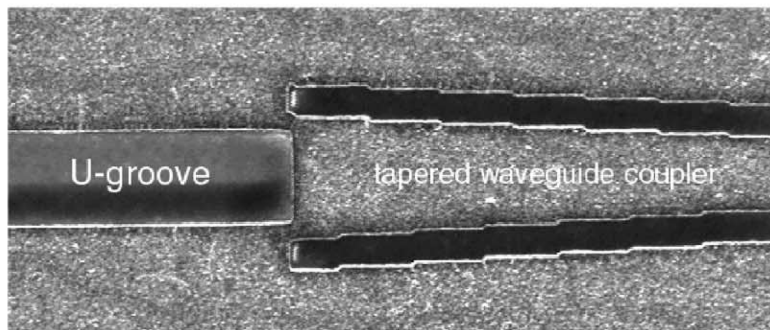

(c)

Fig. 5. (a) Top view of cantilevers with tapered waveguide couplers; (b) SEM micrograph of reactive ion etched silicon/silicon oxide beams; (c) optical image of U groove and the tapered waveguide coupler.

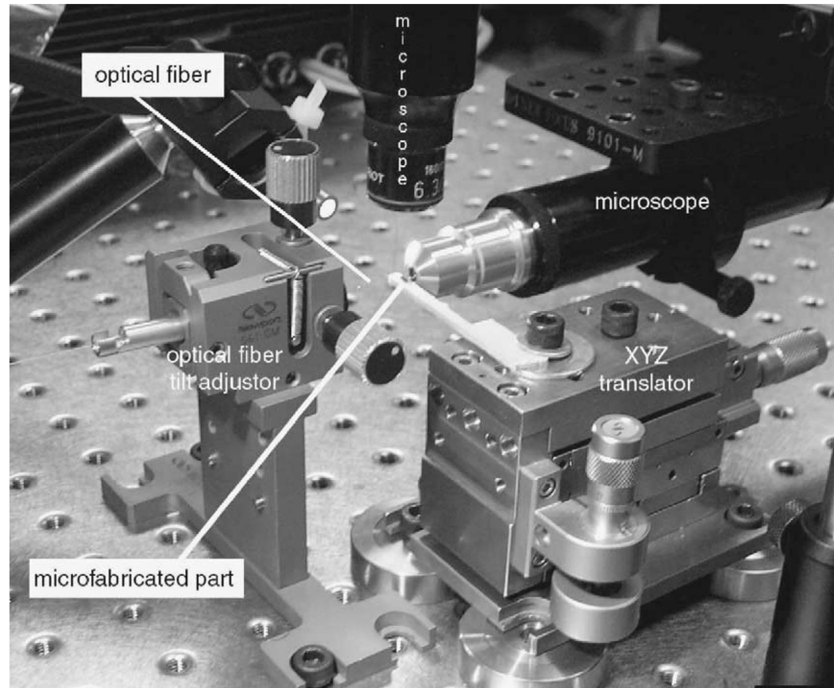

Fig. 6. Optical test apparatus.

(manufactured by APC, dimensions approximately 3 mm × 5 mm, 0.5 mm thick). The piezoelectric bimorph is clamped in a small vise by one of its electrodes, and the outside faces of the bimorph were wired together with a lead. The microfabricated device is placed on the bimorph, and a quick-drying adhesive (Krazy glue (cyanoacrylate adhesive)) was administered (approximately 1 mm in diameter droplet) to the device and bimorph. The glue was allowed a

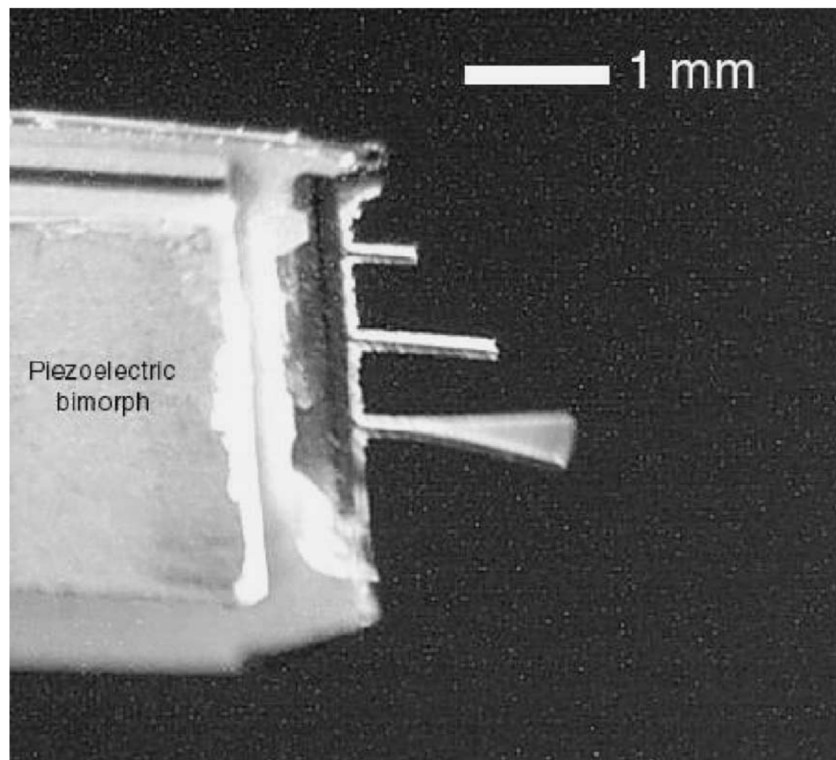

Fig. 7. Piezoelectric bimorph driven at the resonant frequency of the longest cantilever.

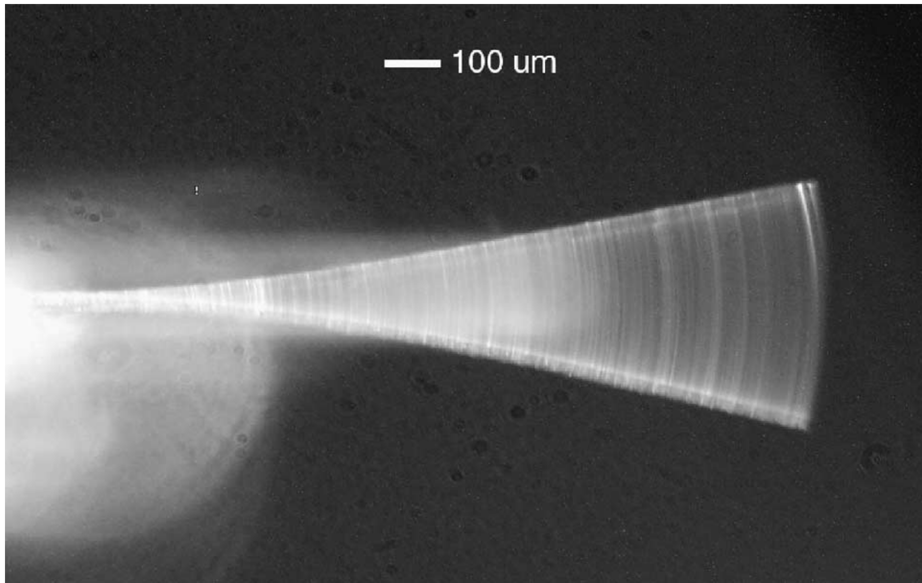

Fig. 8. Representative fiber scanning motion in the first mode of resonance.

minimum of a half-hour to set. The piezoelectric bimorph was driven via a custom-made high voltage amplifier, with a function generator (Stanford Research Systems model DS345) generating a sine wave function. The voltage applied to the bimorph ranged from ± -22 to ± -110 V. Fig. 7 shows a low-magnification view of the microfabricated device attached to the piezoelectric bimorph and driven at the resonant frequency of longest cantilever.

Using one of the microscopes (6.3× or 10× objective, 10× eyepiece), displacement of the tip of the waveguide was measured visually using the eyepiece reticle. This reticle was calibrated using a standard test target pattern. Fig. 8 shows the view of the edge of a microfabricated cantilever driven at resonance. The frequency of the driving function was varied to look for cantilever tip motion, and the maximum amplitude was taken to be indicative of the center frequency. The cantilever beams were vibrated only in one direction, along the thickness dimension (normal to wafer surface).

3. Theory

Deriving the equations of motion for a composite fixed-free cantilever beam allows us to predict the dimensions needed to produce the desired cantilever resonance frequency. For optical scanning applications to work at typical sVGA video rates, we wish the first mode resonance frequency of the cantilever needs to be in excess of 20 kHz.

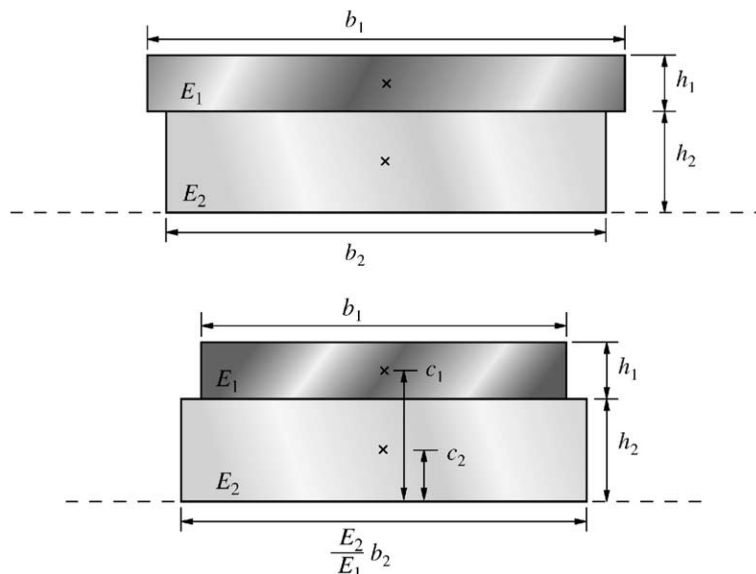

Fig. 9. Original composite beam cross section. Adjusted composited beam cross section using E_1 as the reference elastic modulus.

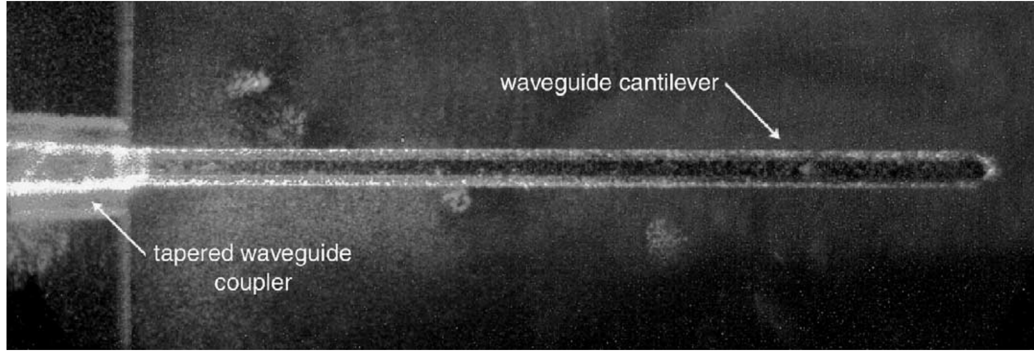

Fig. 10. Top view of optical waveguide cantilever. The length of the beam is 1.5 mm from the support to the tip.

The transverse resonant frequency of a composite beam in a vacuum is [21]

$$f_0 = \frac{1}{2\pi}\left(\frac{1.875}{l}\right)^2\left(\frac{E_{eq}I_{eq}}{\rho_{eq}A_{eq}}\right)^{0.5} \quad (1)$$

where f_0 is the first mode resonant frequency, E_{eq} the equivalent Young's modulus (elastic modulus), I_{eq} the equivalent moment of inertia, ρ_{eq} the equivalent density, A_{eq} the equivalent cross-sectional area (product of width and thickness) and l is the cantilever length.

Where the equivalents of E, I, ρ, and A are found by using the method of composite beams [22]. To compensate for stiffer or more flexible layers of a composite, this method adjusts the geometry (width only) of each of the layers of the composite beam, as illustrated in Fig. 9. This allows one to use the one reference value of Young's modulus (labeled E_1 for this case) for the entire beam by adjusting the beam's geometry to compensate for having a second Young's modulus (E_2). After adjusting the geometry of the beam, the equivalent variables in Eq. (1) are found by the following formulas:

$$\frac{1}{12E_1}\left(\sum_{i=1}^{n} b_i E_i h_i^3\right) + \frac{1}{E_1}\left(\sum_{i=1}^{n} b_i E_i h_i (\bar{c} - c_i)^2\right) \quad (2)$$

where E_i is the Young's modulus of layer i, b_i the width of layer i, h_i the thickness of layer i, and c_i is the centroid of layer i where centroid of the adjusted beam is found by

$$\bar{c} = \frac{\sum_{i=1}^{n} E_i b_i c_i h_i}{\sum_{i=1}^{n} E_i b_i h_i} \quad (3a)$$

The adjusted cross-sectional area is

$$A_{eq} = \frac{1}{E_1}\sum_{i=1}^{n} b_i E_i h_i \quad (3b)$$

The mass density is adjusted to maintain the same mass per unit length:

$$\rho_{eq} = \frac{E_1 \sum_{i=1}^{n} \rho_i b_i h_i}{\sum_{i=1}^{n} E_i b_i h_i} \quad (3c)$$

4. Results

Fig. 10 shows a typical top view of the waveguide cantilever. Note that the bright spots correspond to where light is scattered out of the waveguide. Fig. 11 shows the end of the waveguide emitting light that was coupled using the butt-end coupling technique. Quantitative measurement of optical transmission through the waveguide cantilever was problematic. Since the core of single mode fiber still is larger than our 2 μm thick SiO_2 layer, we placed the light source fiber off-center to avoid the possibility of non-coupled light reaching the optical power meter (Newport 1835-C). Light emanating from only the distal tip of the SiO_2 layer was estimated at 10 nW using the optical power meter. Typically, less than 300 nW is required for applications such as retinal light scanning microdisplays [23]. The low coupling efficiency represents a minimum level of optical transmittance due to the butt-end coupling method and non-planar sides of the cantilever waveguide.

Although no low index buffer layer was used, thus allowing light to exit the SiO_2 layer, we observed that a significant amount of light was scattered out of the waveguide at its side edges. Presumably this is due to non-planar surfaces along the sides of the waveguide. Due to the fact that a low quality lithography mask was used (generated with a 2450 dpi horizontal, 300 dpi vertical printer), features on the tapered waveguide coupler are more staircase-like

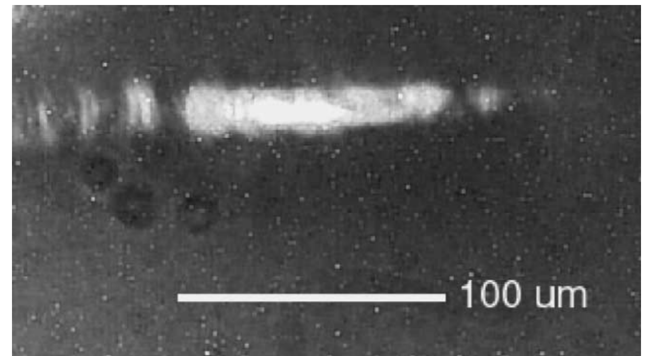

Fig. 11. Light output from waveguide cantilever end.

Table 1
Resonance frequencies of the SiO_2/Si composite levers[a]

Lever no.	Thickness (μm)/width (μm)/length (μm)	Observed resonant frequency (kHz)	Calculated resonant frequency (kHz)	Observed Q factor
1	2.2/97/1500 (SiO_2) 30/84/1500 (Si)	17.19	16.84	N/A
2	2.2/93/1500 (SiO_2) 30/52/1500 (Si)	16.90	16.84	260
3	2.2/97/1500 (SiO_2) 31/50/1500 (Si)	17.77	17.36	296
4	2.2/89/1460 (SiO_2) 35/38/1440 (Si)	20.67	20.82	180
5	2.2/97/1000 (SiO_2) 30/84/1000 (Si)	39.62	37.89	514
6	2.2/92/1000 (SiO_2) 33/56/1000 (Si)	43.10	41.42	540
7	2.2/89/980 (SiO_2) 38/39/980 (Si)	51.50	50.28	396
8	2.2/96/490 (SiO_2) 35/59/490 (Si)	N/A	172.50	N/A

[a] No measurable resonance was found for lever 8.

than linear. This may provide a reasonable explanation for the poor coupling efficiency at the etched end of the tapered waveguide coupler, and for the optical losses along the sides of the waveguide; the supposedly planar surfaces are far from being planar. A non-planar surface to a waveguide allows for angles of incidence which do not result in total internal reflection of light in the waveguide.

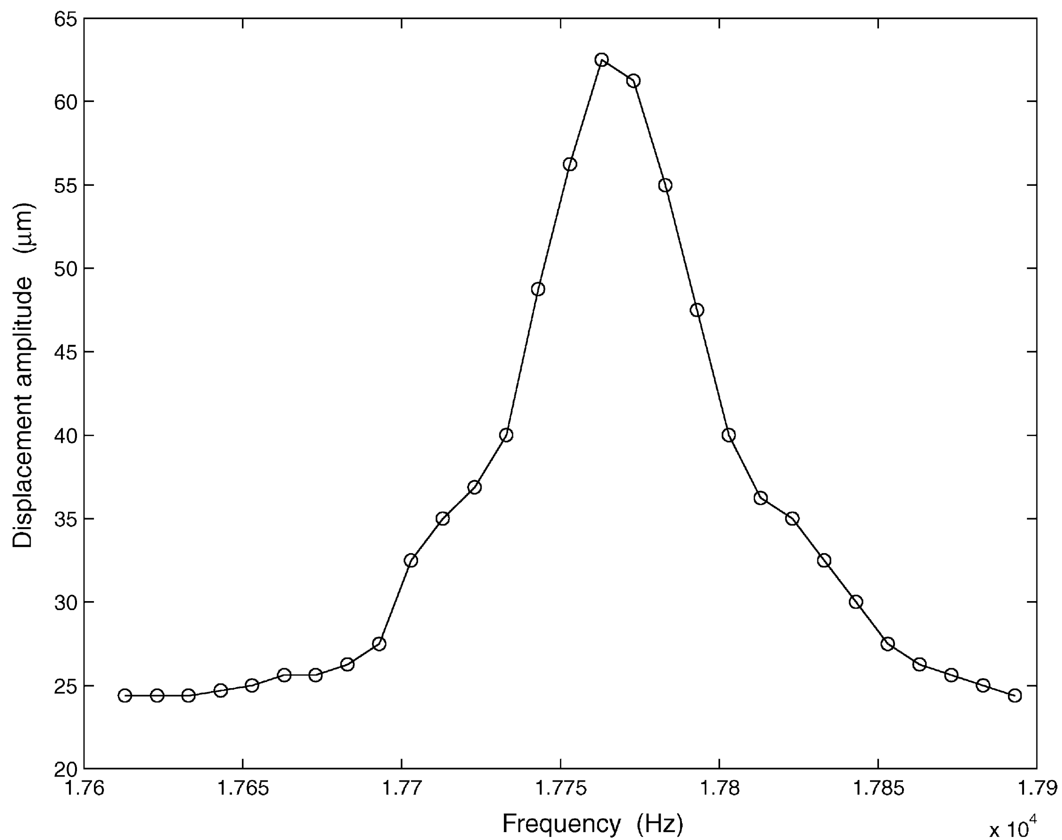

Fig. 12. Amplitude versus frequency of plot of the device reposes of lever number 3 in Table 1.

4.1. Dynamics

The cantilever dimensions were chosen with the criterion that the first mode resonant frequencies should be above 20 kHz. This allows for their use in resonant optical scanning applications at standard video frame rates. While the measured resonant frequencies of the longest cantilevers were slightly short of this goal, good agreement between predicted resonant frequencies from cantilever dimensions and the experimentally measured resonant frequencies was found. The calculated resonant frequency from measured dimensions and the experimentally measured first mode resonant frequency are given in Table 1. The Young's moduli of silicon (125 GPa) and silicon oxide (57 GPa) used for the frequency calculations are based on the values given in [24,25]. The percentage difference from calculated resonant frequencies varied from −0.7 to +4.6%. The amplitude of motion at the tip of the cantilevers for these measurements ranged from 62.5 to 420 μm. *Q* factor values ranged from 180 to 540. An example of the amplitude versus frequency plot of the device reposes is shown in Fig. 12. The beam used here is sample 3 in Table 1.

5. Conclusions

We have demonstrated a SiO_2/Si optical waveguide lever for use as a micro-optical scanner. A novel double-sided micromachining process for the device fabrication has been developed that allows the use of capacitively coupled RIE equipment for high aspect ratio etching. The resulting etch rates in Si of 2.0–2.2 μm/min are comparable to 1–3 μm/min from the standard ICP deep ion etching process. Although a lower anisotropy (∼0.5) and lower selectivity to thermal oxide ($Si:SiO_2 = 10:1$) and to photoresist ($Si:+PR = 8.6:1$) resulted, the proposed process is much simpler and only requires only use of an aluminum mask.

The most problematic aspect of this work was estimating optical waveguiding efficiency. For a variety of reasons, including possible "rough" surfaces where light was to be coupled via a single mode optical fiber, we did not use the U-shaped groove for holding the singlemode illumination fiber. Instead, the silicon block was cleaved so that it left a cleaved surface at some point along the tapered waveguide coupler. Low coupling efficiency was attributed to the lack of low index buffer layer, butt-end coupling, and the non-planar waveguide surfaces.

In terms of dynamics, the cantilever beams possessed first mode resonance frequencies in good agreement with predicted values. Errors between observed and calculated resonance frequencies ranging from 17 to 51 kHz were within 5.0%. For one-dimensional scanning, the 2 μm waveguide tip forms a 2 μm-sized pixel under ideal imaging conditions, resulting in up to 200 pixels in the linear FOV at our largest displacement of 0.4 mm. Though initially the dynamics tests were performed only in one dimension of actuation, future design work and testing will incorporate two-dimensional scanning. Future efforts will also include reduction of both dimensions of the cross-sectional area of the waveguide to produce a smaller and a more square shape illumination source at the end of the waveguide cantilever tip.

Acknowledgements

This work was supported in part by grants given to Dr. Seibel by the Washington Technology Center and The Whitaker Foundation. The financial support of the Washington Technology Center Research Fund is gratefully acknowledged.

References

[1] E.J. Seibel, Q.J. Smithwick, C.M. Brown, P.G. Reinhall, Single fiber flexible endoscope: general design for small size, high resolution, and wide field of view, in: Proceedings of the EOS/SPIE EUROPTO on Biomonitoring and Endoscopy Technologies, vol. 4158, pp. 29–39.

[2] C.M. Brown, M. Fauver, P.G. Reinhall, E.J. Seibel, Mechanical design and analysis for a scanning fiber endoscope, in: Proceedings of the International Mechanical Engineering Congress and Exposition, New York, NY, November 11–16, 2001.

[3] L. Giniuanas, R. Juskaitis, S.V. Shatalin, Endoscope with optical sectioning capability, Appl. Opt. 32 (16) (1993) 2888–2890.

[4] D.L. Dickensheets, G.S. Kino, A scanned optical fiber confocal microscope, Proc. SPIE 2184 (39) (1994) 39–47.

[5] U. Hofmann, S. Mehlmann, M. Witt, K. Dorschel, R. Schutz, B. Wagner, Electrostatically driven micromirrors for a miniaturized confocal laser scanning microscope, SPIE Conf. Miniat. Syst. Microopt. MEMS 3878 (1999) 29–38.

[6] D.L. Dickensheets, G.S. Kino, Micromachined scanning confocal optical microscope, Opt. Lett. 21 (10) (1996) 764–766.

[7] E.D. Palik, Handbook of Optical Constants of Solids, Academic Press, New York, 1985.

[8] R.D. Jolly, R.S. Muller, Miniature cantilever beams fabricated by anisotropic etching of silicon, J. Electrochem. Soc. 127 (1980) 2750.

[9] S. Wang, V.M. McNeil, M.A. Chmidt, An etch-stop utilizing selective etching of N-type silicon by pulse potential anodization, J. Microelectromech. Syst. 1 (4) (1992) 187–192.

[10] K.E. Petersen, Micromechanical light modulator array fabricated on silicon, Appl. Phys. Lett. 31 (1977) 521.

[11] W. Choi, J.G. Smits, A method to etch a undoped silicon cantilever beams, J. Microelectromech. Sys. 2 (2) (1993) 82–86.

[12] A.V. Churenkov, Silicon micromechanical optical waveguide for sensing and modulation, Sensor. Actuators A 57 (1996) 21–27.

[13] K. Burcham, G. De Brabander, J. Boyd, Micromachined silicon cantilever beam accelerometer incorporating an integrated optical waveguide, SPIE Integ. Opt. Microstruc. 1973 (1992) 12–17.

[14] R. Toda, K. minami, M. Esashi, Thin beam bulk micromachining based on RIE and xenon difluoride silicon etching, Sens. Actuators A 66 (1998) 268–272.

[15] A. Chand, M.B. Biani, T. Schaffer, P. Hansma, Microfabricated small metal cantilevers with silicon tip for atomic force microscope, J. Microelectromech. Syst. 9 (1) (2000) 112–116.

[16] T. Eng, S. Kan, G. Wong, Voltage-controlled micromechanical SOI optical waveguides, in: Proceedings of the IEEE Region 10th International Conference on Microelectronics and VLSI (Asia-Pacific Microelectronics 2000), 1995, pp. 195–197.

[17] E.A. Irene, R. Ghez, Silicon oxidation studies: the role of H_2O, J. Electrochem. Soc. 124 (11) (1977) 1757–1761.
[18] M.V. Whelan, A.H. Geomans, L.M.C. Goossens, Residual stresses at an oxide–silicon interface, Appl. Phys. Lett. 10 (10) (1967) 262–264.
[19] W.-C. Wang, J. Ho, P. Reinhall, Deep reactive ion etching of silicon using aluminum as etching mask, SPIE OPTO (Ireland), 2002, in press.
[20] S. Vogel, U. Schaber, K. Kuhl, R. Schafflik, H. Padel, F. Kozlowski, B. Hillerich, Novel microstructuring technologies in silicon, microsystem technologies 98, in: Proceedings of the Sixth International Conference on Micro, Electro, Opto, Mechanical Systems and Components, VDE, Berlin, 1998, pp. 427–432.
[21] J.P. Den Harttog, Mechanical Vibrations, MacGraw-Hill, New York, 1956.
[22] A.C. Ugura, S. Fenster, Advanced Strength and Applied Elasticity, Prentice-Hall, Upper Saddle River, 1995, pp. 207–212.
[23] R.S. Johnston, S.R. Willey, Development of a commercial retinal scanning display helmet and head-mounted displays and symbology design requirements II, Proc. SPIE 2465 (1995) 2–13.
[24] B. Bhushan, X. Li, Micromechanical and tribological characterization of doped single-crystal silicon and polysilicon films for microelectromechnical systems devices, J. Mater. Res. 12 (1997) 54–64.
[25] K.E. Petersen, Dynamic micromechanics on silicon: techniques and devices, IEEE Trans. Electron Devices 25 (10) (1978) 1249.

Biographies

Wei-Chih Wang obtained his PhD in Electrical Engineering from University of Washington in 1996. He is currently a lecturer in the Department of Mechanical Engineering, University of Washington. His research interests are MEMS and Fiber-Optic Sensor Technology.

Mark Fauver received the BS degree in Physics from University of California, Los Angeles, in 1993, and the MS degree in Bioengineering from University of Washington, Seattle, in 1996. Currently he is working works as a Research Engineer in the Human Interface Technology Laboratory at University of Washington, specializing in Microfabricated Device Design and Implementation.

Joe Nhut Ho is currently working towards his MS in Mechanical Engineering at the University of Washington, Seattle. His research interests are in the area of Fluid Mechanics.

Eric J. Seibel received his BS from Cornell University, Ithaca, NY in 1983, his MS in Mechanical Engineering from the University of California, Berkeley, CA in 1984, and his PhD in Bioengineering after working in the medical device industry for 4 years, from the University of Washington, Seattle, WA in 1996. Currently he is an Assistant Research Professor in Mechanical Engineering at the University of Washington, Seattle. His research interests are microfabrication of optical scan systems for image acquisition and display for biomedical applications.

Per G. Reinhall received his PhD from California Institute of Technology in 1982. Currently he is Professor in Mechanical Engineering at the University of Washington, Seattle. His main research interests are in the areas of non-linear dynamics and structural acoustics. He is also involved in System Identification, Stochastic Processes, and Computational Methods applied to Elasticity and Plasticity.